ACS NANO

www.acsnano.org

Open Access

This article is licensed under CC-BY 4.0

ARTICLE

Direct Imaging of Carrier Funneling in a Dielectric Engineered 2D Semiconductor

Nicolas Gauriot, Arjun Ashoka, Juhwan Lim, Soo Teck See, Jooyoung Sung, and Akshay Rao*

Cite This: *ACS Nano* 2024, 18, 264–271

Read Online

ACCESS | Metrics & More | Article Recommendations | Supporting Information

ABSTRACT: In atomically thin transition-metal dichalcogenides (TMDCs), the environmental sensitivity of the strong Coulomb interaction offers promising approaches to create spatially varying potential landscapes in the same continuous material by tuning its dielectric environment. Thus, allowing for control of transport. However, a scalable and CMOS-compatible method for achieving this is required to harness these effects in practical applications. In addition, because of their ultrashort lifetime, observing the spatiotemporal dynamics of carriers in monolayer TMDCs, on the relevant time scale, is challenging. Here, we pattern and deposit a thin film of hafnium oxide (HfO_2) via atomic layer deposition (ALD) on top of a monolayer of WSe_2. This allows for the engineering of the dielectric environment of the monolayer and design of heterostructures with nanoscale spatial resolution via a highly scalable postsynthesis methodology. We then directly image the transport of photoexcitations in the monolayer with 50 fs time resolution and few-nanometer spatial precision, using a pump probe microscopy technique. We observe the unidirectional funneling of charge carriers, from the unpatterned to the patterned areas, over more than 50 nm in the first 20 ps with velocities of over 2×10^3 m/s at room temperature. These results demonstrate the possibilities offered by dielectric engineering via ALD patterning, allowing for arbitrary spatial patterns that define the potential landscape and allow for control of the transport of excitations in atomically thin materials. This work also shows the power of the transient absorption methodology to image the motion of photoexcited states in complex potential landscapes on ultrafast time scales.

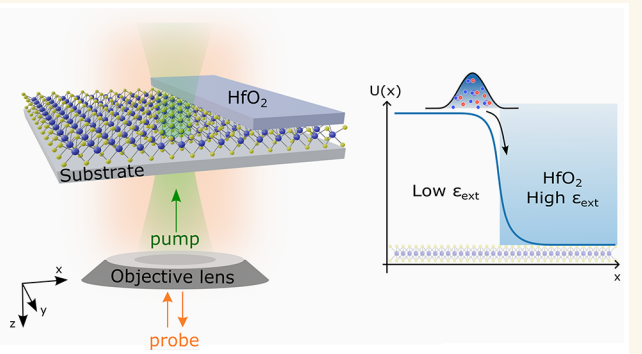

KEYWORDS: *two-dimensional materials, microscopy, transient absorption, transition-metal dichalcogenides, transport, excitons*

Downloaded via DAEGU GYEONGBUK INST SCI & TECHLGY on February 1, 2024 at 16:11:37 (UTC).
See https://pubs.acs.org/sharingguidelines for options on how to legitimately share published articles.

Controlling the transport of electronic excitations is central to semiconductor technologies. To this end, several strategies have been developed to tailor the band structure of materials on the nanoscale. This includes spatial variations in the material stoichiometry,[1] strain gradients,[2] or the formation of a heterojunction with different materials.[3]

Compelling opportunities in band structure design have appeared with the advent of two-dimensional (2D) semiconductors. Because they are atomically thin, they are very sensitive to their environment. For example, strain,[4−14] environmental dielectric screening,[15−25] polarization of ferroelectric substrate,[26,27] and adsorption of chemicals on the surface[28,29] have been shown to have a significant impact on the energetics of the material. This offers the possibility to generate complex potential landscapes, postsynthesis and in the same material, by engineering the material's surroundings.[8,11,14,15,20,26,27,30,31]

Among 2D semiconductors, monolayer (ML) transition-metal dichalcogenides (TMDCs), are particularly promising for optoelectronic applications thanks to the combination of direct bandgaps, large carrier mobilities, and strong light−matter interaction.[32−35] The optical response of a ML TMDC is dominated by excitons because of an unusually strong Coulomb interaction.[36,37] The origin of this strong Coulombic interaction is well understood. The electrostatic potential of a charge is screened more or less effectively, depending on the permittivity of the medium in which it is embedded in. For an atomically thin material, this includes the surrounding media, which is usually a low-dielectric material (typically air). The screening of the Coulomb interaction is therefore much lower than in bulk inorganic semiconductors. This also means that the electron−hole interaction and the electron−electron

Received: June 30, 2023
Revised: November 23, 2023
Accepted: December 1, 2023
Published: December 18, 2023

© 2023 The Authors. Published by American Chemical Society

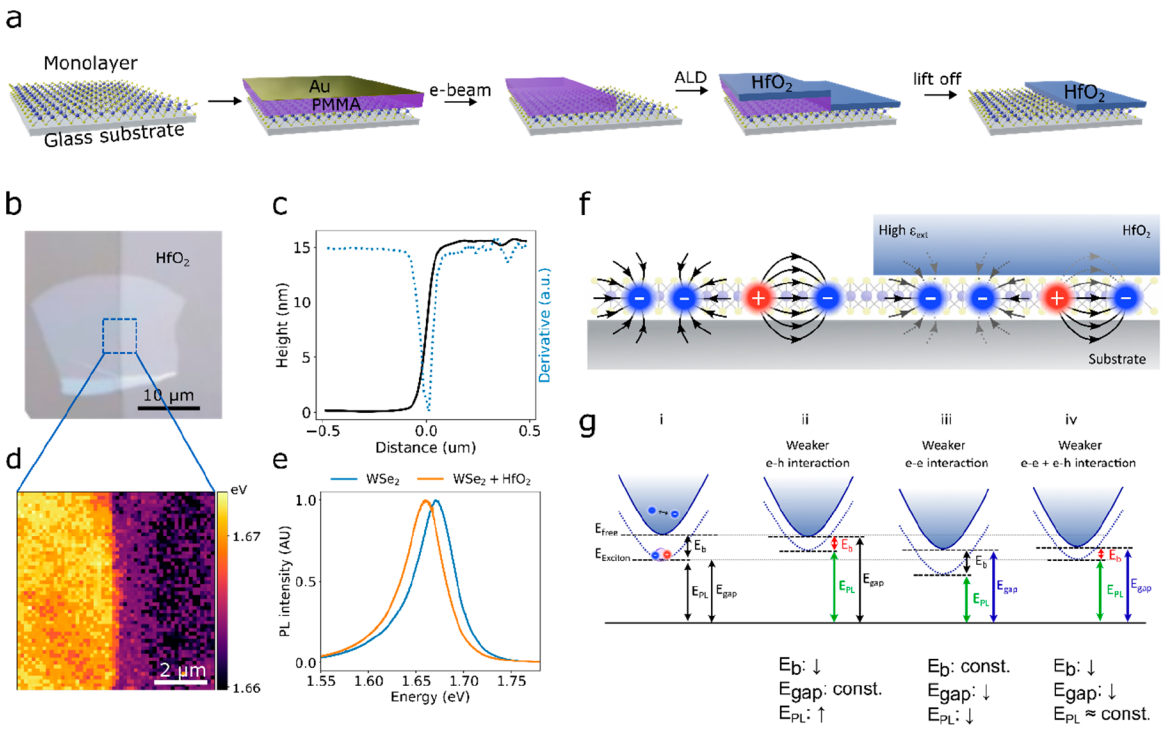

Figure 1. Coulomb engineering in monolayer WSe_2. (a) Schematic of the heterostructure fabrication process. (b) Micrograph of a representative sample. (c) AFM height profile (black) and its derivative (blue) across the junction. (d) Map of the transition energy extracted from PL spectra. (e) Representative photoluminescence spectra on each side of the junction. (f) Schematic of the sample architecture. (g) Schematic of the energy levels and the effect of the different interaction terms on the different electronic transitions (see main text for details).

interaction depend on the dielectric constant of the surrounding media.[15−19,21,22,38] Consequently, both the quasiparticle bandgap and the exciton binding energy can be tuned by engineering the local dielectric environment.

Although the consequences of strain gradients on excitonic transport have been extensively studied,[6,8,11,13,14,39−43] the full possibilities offered by dielectric engineering remain underexplored. Specifically, two experimental challenges must be overcome. First, we need scalable ways to pattern the dielectric environment over large areas, rather than simply exfoliating and stacking small areas of arbitrarily shaped graphene or h-BN onto the 2D material to be engineered, as has been done to date. Second, we require tools to understand the dynamics and transport of photoexcitation in these complex potential landscapes. This has been challenging to date, as most studies rely on photoluminescence (PL) microscopy, which lacks both the ultrafast time resolution and the nanoscale spatial precision to study these phenomena on the relevant spatiotemporal scales. Furthermore, PL is insensitive to dark excitons and charges, both of which play major roles in these materials.

Here, we tackle both of these issues and demonstrate the patterning of a WSe_2 monolayer with atomic layer deposition, which in principle allows for arbitrary spatial patterns via a highly scalable methodology. We use this method to pattern areas covered with HfO_2, a high-dielectric-constant insulating material which significantly alters the dielectric environment around the WSe_2 monolayer. Then, using fs-transient optical absorption microscopy, we directly image the motion of carriers, with high temporal resolution and spatial precision well below the diffraction limit. We observe the unidirectional funneling of charge carriers, from the unpatterned to the patterned areas, over more than 50 nm in the first 20 ps after photoexcitations, with velocities over 2×10^3 m/s at room temperature.

RESULTS AND DISCUSSION

Figure 1b shows a micrograph of a representative sample: a monolayer of WSe_2 partially covered by a 15 nm thick HfO_2 film. We chose HfO_2 for its high dielectric constant ($\varepsilon \approx 25$),[44] and its wide use as a gate oxide in CMOS-compatible technologies. Here, the HfO_2 patch is patterned by e-beam lithography and deposited by ALD as described in detail in Figure 1a. Figure 1c presents an AFM height profile of the junction and its derivative, with a fwhm of ∼50 nm, illustrating the sharpness of the junction (a full AFM map of the junction is presented in Supplementary Note 1). Notably, unlike methods relying on the stamping of materials on the 2D layer, this process is highly scalable and could be easily extended to generate more complex patterns.

In order to understand the effect of the high-dielectric environment on the electronic structure of WSe_2, we performed scanning confocal photoluminescence (PL) measurements on both the pristine WSe_2 monolayer and the WSe_2/HfO_2 stack. Representative PL spectra from each side of the junction are presented in Figure 1e. We then extract the energy of the optical gap from the PL spectra obtained over the junction and retrieve the 2D map of the transition energy, as shown in Figure 1d. We observe a clear 17 meV red shift of the excitonic transition on the HfO_2-covered side compared to the pristine layer.

Since HfO_2 has a large dielectric constant, the screening of the electron−hole interaction in WSe_2 is more effective on the side covered by HfO_2, which reduces the binding energy and blue-shifts the exciton transition (Figure 1g(ii). At the same

https://doi.org/10.1021/acsnano.3c05957
ACS Nano 2024, 18, 264−271

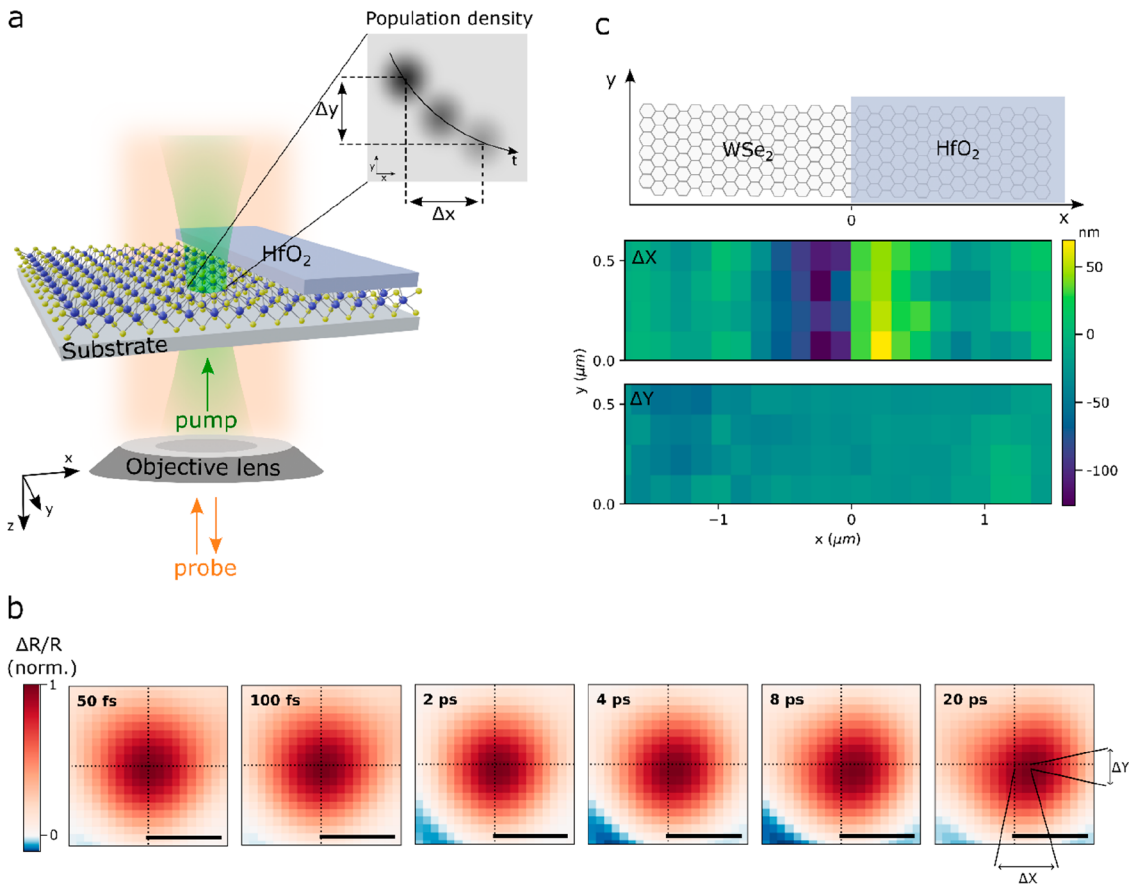

Figure 2. Imaging of the ultrafast transport. (a) Schematic of the pump−probe microscopy experiment. See main text for details. (b) Time evolution of the transient reflection signal after excitation at a representative point near the boundary. (c) Map of the extracted shifts of the excited state population in the direction perpendicular to the junction (ΔX) and parallel to the junction (ΔY) after a 5 ps delay, as a function of the excitation position. The boundary is located at $x = 0$ as illustrated in the top panel.

time, since the electron−electron interaction is also weaker, the bandgap is reduced. This red-shifts the transition (Figure 1g(iii). Based on previous experimental and theoretical work, we expect the decrease in quasiparticle gap and in the exciton binding energy, on the HfO_2-covered side, to be of similar magnitude and on the order of 100 meV.[15,21,25,45] These two opposite effects almost cancel each other, and in the end, the optical gap is only modified by a small amount (Figure 1g(iv)). We note that the sharp shift in the optical gap is observed only after annealing the sample (see Methods). Prior to annealing, we also observe a red shift of the PL on the HfO_2-covered flake; however the shifts are larger and not homogeneous and the transition from pristine to covered flake is not sharp (see Supplementary Note 2). This suggests that the ALD process induces strain in the monolayer leading to additional shifts of the optical gap.[46] Thermal annealing relaxes strain, and a sharp in-plane junction that strictly follows the HfO_2 patch is created.

To image the transport of excitations in this asymmetric potential landscape, we use a transient reflection microscopy technique. Figure 2a presents a schematic of the experiment. Briefly, a 15 fs pump pulse, focused near the diffraction limit, generates a population of excited states. After a controllable time delay, the transient reflection of the sample is imaged onto a camera with a wide-field probe pulse. More details on the experimental setup are presented in Methods and elsewhere.[47,48] In contrast to PL-based imaging, our technique is sensitive to both bright and dark states, and because it relies on optical gating, it exhibits a much faster time resolution. As previously described, differential imaging allows tracking the population of photoexcitations in the material, in time and space, with 50 fs time resolution and few-nanometer precision.[47,48] Figure 2b shows the evolution of the transient reflection ($\Delta R/R$) images obtained after exciting the sample at a representative point near the junction where we can clearly see the movement over time of the center of mass of the $\Delta R/R$ signal.

In order to quantify this motion, we extract the position of the excited state distribution ($X(t)$, $Y(t)$) at each time delay by fitting these images with a 2D Gaussian distribution, and we measure the movement of the distribution in the direction perpendicular ($\Delta X(t) = X(0) - X(t)$) and parallel ($\Delta Y(t) = Y(0) - Y(t)$) to the junction as illustrated in the inset of Figure 2a. To study how this motion varies depending on where the excitations are launched (i.e., the position at $t = 0$), we repeat this experiment at various points around the junction. For each starting position ($X(0)$,$Y(0)$) we extract the ΔX and ΔY shifts after a 5 ps delay to build up the maps presented in Figure 2c. We observe no significant shift (ΔY) of the mean of the distribution in the direction parallel to the junction irrespective of the excitation position, while in the perpendicular direction (ΔX), we measure clear positive and negative shifts for the starting position in the vicinity of the junction. This observation of opposite ΔX shifts on each side of the junction paints a slightly more complex situation than a simple

https://doi.org/10.1021/acsnano.3c05957
ACS Nano 2024, 18, 264−271

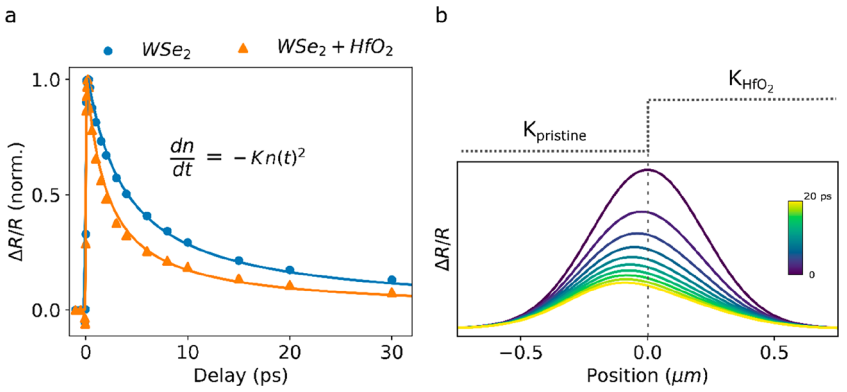

Figure 3. Effect of the spatially varying kinetics. (a) Decay kinetics of the $\Delta R/R$ signal far from the boundary on the pristine side (blue dots) and the HfO_2-covered side (orange triangles). Solid lines are fits to a bimolecular decay, describing exciton−exciton annihilation. (b) Simulated Gaussian profile decaying through a bimolecular decay with a spatially dependent decay rate. The decay rate follows the step function illustrated in the top panel with values of K_{WSe_2} and K_{HfO_2} extracted from (a). The profiles are convoluted with a Gaussian to simulate the point spread function of the microscope.

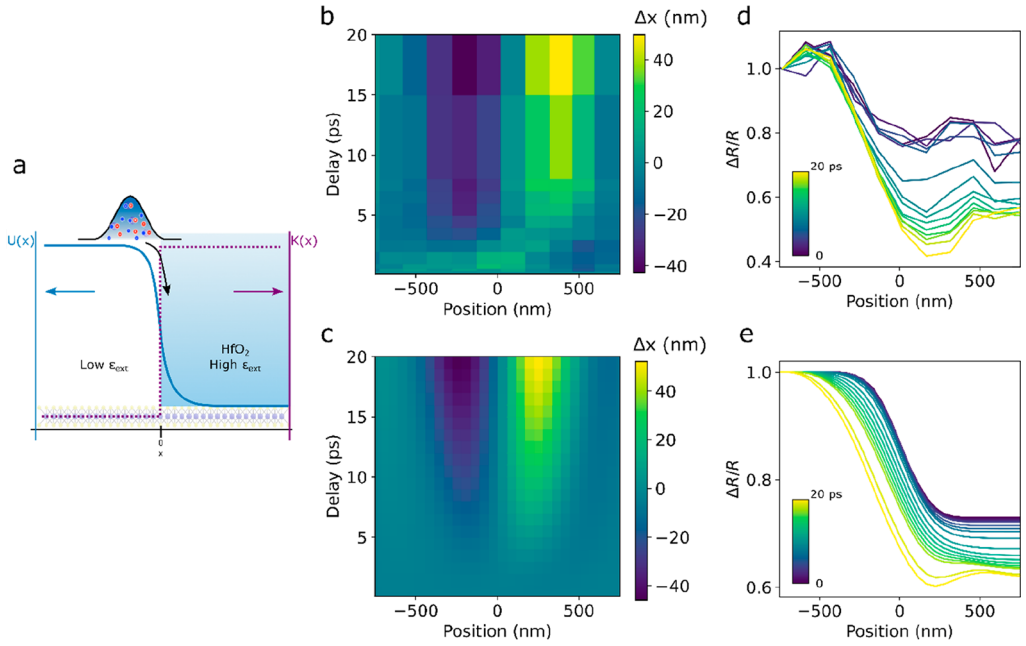

Figure 4. Unidirectional exciton funnelling. (a) Schematic of the modeled potential step U and annihilation rate K across the junction. (b) Map of the ΔX shift as a function of time and excitation position near the junction. (c) Corresponding simulated map. (d) Temporal variation of $\Delta R/R$ corresponding to the map in (b). (e) Corresponding simulated $\Delta R/R$.

unidirectional funneling of excitations across the junction, and a more detailed analysis is required before conclusions on transport can be drawn.

To understand the origin of these opposite ΔX shifts, we measure the decay dynamics on each side of the junction far from the boundary. As shown in Figure 3a, the two kinetics are well approximated by a bimolecular decay, with a decay rate $k_{HfO_2} = 1.7 \times 10^{-2}$ cm^2 s^{-1} on the covered side and $k_{pristine} = 0.9 \times 10^{-2}$ cm^2 s^{-1} on the pristine side. This is consistent with previous studies showing that the decay dynamics in TMDC monolayers are dominated by an efficient exciton−exciton annihilation.[49−51] Since the $\Delta R/R$ signal decays faster on the HfO_2 side than on the pristine side, in the absence of any transport, a Gaussian distribution sitting across the junction will appear to move toward the pristine side ($\Delta X < 0$), as illustrated in Figure 3b. This means that the negative shifts do not reflect a movement of the population but rather a change in its spatial profile due to the underlying difference in the decay dynamics on either side of the junction. The measured spatial shifts are therefore due to a combination of two effects: actual transport of excitons in the monolayer and a spatial variation of the decay dynamics. Consequently, the raw ΔX shifts presented here are smaller than the true motion of the excitations in the monolayer. More generally, the raw spatial shifts measured in time-resolved microscopy experiments similar to that presented here (whether based on pump−probe or photoluminescence signals) should not be interpreted as movement of carriers in the material without a spatially resolved analysis of the decay dynamics.

In order to evaluate the actual transport of excitations in the monolayer, we modeled the spatiotemporal evolution of the excited state population across the junction with a drift diffusion model. Considering the excitons as quasiparticles evolving in a potential landscape $U(x)$ and decaying through a

https://doi.org/10.1021/acsnano.3c05957
ACS Nano 2024, 18, 264−271

bimolecular recombination with spatially varying decay rate $k(x)$, the exciton population $n(r,t)$ is described by the equation

$$\frac{\partial n}{\partial t} = D\nabla^2 n(t) + \frac{D}{k_B T}\nabla(n(t)\nabla U) - k(x)n^2(t)$$

where D is the diffusion coefficient in the monolayer. We model U as a smooth step function, $U(x) = \frac{U_0}{2}\left\{1 - \mathrm{erf}\left(\frac{x}{\sqrt{2}\sigma}\right)\right\}$, where erf is the error function, such that ∇U is a Gaussian of variance σ, while $k(x) = k_{\mathrm{pristine}} + H(x)\{k_{\mathrm{pristine}} - k_{\mathrm{HfO_2}}\}$, with H being the Heaviside step function, as illustrated in Figure 4a. Importantly, we fix the annihilation rate k_{pristine} and $k_{\mathrm{HfO_2}}$ to the values extracted from Figure 3. Next, we model the initial exciton distribution as a Gaussian such that $n(r, 0) = Ae^{-\left(\frac{x-X(0)}{\sigma_0}\right)^2}$, and to simulate the microscope objective point spread function (PSF) the calculated $n(r,t)$ distribution is convolved with another Gaussian, PSF $= e^{-\left(\frac{x-X(0)}{\sigma_0}\right)^2}$. Finally, we extract the position $X(t)$ of the simulated distribution with the same analysis as that with the measured data described before. Figure 4 compares the measured and simulated data. Figure 4b shows a map of the measured ΔX shift as a function of time and initial position around the junction. Figure 4d presents the time evolution of the amplitude of the measured $\Delta R/R$ signal at the same positions. Figure 4c,e shows the corresponding simulation results, in good agreement with the experimental results, for $D = 2$ cm^2/s, $U_0 = 150$ meV, and $\sigma = 55$ nm. This simple model therefore confirms the funneling and unidirectional motion of excitations from the pristine side to the HfO_2-covered side of the junction. We note that varying D from 0.1 to 10 cm^2/s but keeping the drift current $J = D/k_BT\ \nabla(n(t)\nabla U)$ constant (i.e., keeping DU_0 constant) does not affect the simulation results significantly (see Supplementary Note 3). This suggests that for the time scale studied here (<20 ps) the effect of the diffusion term is negligible compared to the drift current.

The optical pump used here is centered at 550 nm (2.25 eV) and is well above the free particle gap of monolayer WSe_2. The pump fluence is 17 μJ/cm^2, which with an absorption of 10%[52] leads to 4×10^{12}/cm^2 absorbed photons. Under these conditions, mid-infrared pump probe spectroscopy measurements revealed that excitons form within few hundreds of fs, but about 40% of excitations remain as unbound electrons and holes.[53]

Reported values of diffusion coefficients for excitons in monolayer TMDC range from $D = 0.1$ cm^2/s to $D = 10$ cm^2/s.[49,54−58] However, even if we assume the largest diffusion constant, a potential step $U_0 = 30$ meV is required to match the experimental data, and the 17 meV potential step of the excitons, which is lower than the thermal energy ($k_BT \approx 25$ meV), is too small to drive the observed motion across the junction. Free charges, however, with a potential step across the junction given by the change in quasiparticle gap of about 100 meV are more likely to be driving this motion. Reported mobilities in TMDC are on the order of 100 V cm^2/s,[33,59] which leads to the diffusion coefficient $D \approx 2.5$ cm^2/s, bringing U_0 to 120 meV, in good agreement with the expected change in the free particle gap across the junction.

CONCLUSION

To summarize, by making use of the sensitivity to the dielectric environment of monolayer TMDC, we have engineered monolayer WSe_2. We have observed a unidirectional flow of excitations through the junction from the unpatterned to the patterned areas, with shifts of the mean position of excitation higher than 50 nm in 20 ps, leading to a lower bound for the carrier velocity of 2.5×10^3 m/s. This simple proof of concept showcases the opportunity offered by 2D semiconductors to engineer potential landscapes to direct excitations and reveals the power of transient absorption microscopy as a technique to observe energy flows in materials on an ultrafast time scale.

METHODS

Sample Preparation. Monolayers of WSe_2 were exfoliated from bulk crystal (HQgraphene) on PDMS films (TELTEC) and transferred on a 170 nm thick glass substrate with a dry transfer technique.[60] Electron beam lithography was used to pattern the HfO_2 film. 15 nm of gold was evaporated on top of the PMMA resist to act as a discharge layer during the lithography and etch after exposure (gold etchant standard, Sigma-Aldrich). A 15 nm film of HfO_2 was then grown with atomic layer deposition (125 °C, $HfCl_4$ and H_2O precursors) before lift-off in acetone. The samples were subsequently annealed in at 200 °C in partial vacuum for 2 h to relax strain.

Transient Absorption Microscopy. Our pump−probe microscopy setup was described previously.[47,48] Here, a pump pulse (centered at 550 nm, fluence 17 μJ/cm^2) is focused onto the sample with an oil immersion objective (NA = 1.1) to produce a near-diffraction-limited local photoexcitation. After a variable time delay, a copropagating wide-field probe pulse (750 nm, ∼20 μm full width at half-maximum) is reflected on the sample and imaged onto an emCCD camera (Rolera Thunder, QImaging). Wide-field probe images in the presence and absence of the pump excitation are recorded by chopping the pump pulse at 40 Hz. The pump and probe pulses are derived from a Yb:KGW amplifier (1030 nm, 5 W, 200 kHz, 200 fs, LightConversion) via white-light continuous generation and subsequent spectral filtering and compression with chirped mirrors. After transmission through the objective and the glass substrate, the pump is 13 fs, while the probe is 7 fs before the objective. At the sample the probe is significantly chirped, and integrating the signal over a 10 nm spectral bandwidth gives a 50 fs temporal resolution as demonstrated previously.[47]

Microphotoluminescence. PL spectroscopy was performed on a Renishaw Invia confocal setup equipped with a motorized piezo stage, using an air-cooled Ar-ion 514.5 nm continuous wave (CW) laser via a 100× objective (NA = 0.9).

ASSOCIATED CONTENT

Data Availability Statement

The data underlying all figures in this article are publicly available from the University of Cambridge repository at (https://doi.org/10.17863/CAM.104577).

Supporting Information

The Supporting Information is available free of charge at https://pubs.acs.org/doi/10.1021/acsnano.3c05957.

AFM height map of the heterostructure, map of the transition energy extracted from PL spectra for a nonannealed sample, and comparison of different simulation results (PDF)

AUTHOR INFORMATION

Corresponding Author

Akshay Rao − *Cavendish Laboratory, University of Cambridge, CB3 0HE Cambridge, United Kingdom;*

https://doi.org/10.1021/acsnano.3c05957
ACS Nano 2024, 18, 264−271

orcid.org/0000-0003-4261-0766; Email: ar525@cam.ac.uk

Authors

Nicolas Gauriot − *Cavendish Laboratory, University of Cambridge, CB3 0HE Cambridge, United Kingdom;* orcid.org/0000-0001-7725-7208

Arjun Ashoka − *Cavendish Laboratory, University of Cambridge, CB3 0HE Cambridge, United Kingdom*

Juhwan Lim − *Cavendish Laboratory, University of Cambridge, CB3 0HE Cambridge, United Kingdom*

Soo Teck See − *Cavendish Laboratory, University of Cambridge, CB3 0HE Cambridge, United Kingdom*

Jooyoung Sung − *Cavendish Laboratory, University of Cambridge, CB3 0HE Cambridge, United Kingdom; Department of Physics and Chemistry, DGIST, Daegu 42988, Republic of Korea*

Complete contact information is available at: https://pubs.acs.org/10.1021/acsnano.3c05957

Funding

This work was funded by the UKRI. For the purpose of open access, the author has applied a Creative Commons Attribution (CC BY) license to any Author Accepted Manuscript version arising.

Notes

The authors declare no competing financial interest.

ACKNOWLEDGMENTS

N.G. thanks S. Haws, T. Sharp, and R. Beadle for technical support. J.S. acknowledges support from the Basic Science Program through the National Research Foundation of Korea (NRF-2022R1C1C1005970) and DGIST Start-up Fund (20230348) Program funded by the Ministry of Science and ICT. The ALD was performed on the Royce Cluster Tool, part of the Cambridge Henry Royce Institute equipment, Grant No. EP/P024947/1, with equipment procured by Sir Henry Royce Institute—recurrent Grant No. EP/R00661X/1. This work has received funding from the European Research Council under the European Union's Horizon 2020 research and innovation programme (grant agreement number 758826). This work has received funding from the Engineering and Physical Sciences Research Council (UK).

REFERENCES

(1) Virshup, G. F.; Ford, C. W.; Werthen, J. G. A 19% Efficient AlGaAs Solar Cell with Graded Band Gap. *Appl. Phys. Lett.* **1985**, *47* (12), 1319−1321.

(2) Minot, E. D.; Yaish, Y.; Sazonova, V.; Park, J. Y.; Brink, M.; McEuen, P. L. Tuning Carbon Nanotube Band Gaps with Strain. *Phys. Rev. Lett.* **2003**, *90* (15), 4.

(3) Capasso, F. Band-Gao Engineering: From Physics and Materials to New Semiconductor Devices. *Science* **1987**, *235* (4785), 172−176.

(4) Roldán, R.; Castellanos-Gomez, A.; Cappelluti, E.; Guinea, F. Strain Engineering in Semiconducting Two-Dimensional Crystals. *J. Phys.: Condens. Matter* **2015**, *27* (31), 313201.

(5) He, K.; Poole, C.; Mak, K. F.; Shan, J. Experimental Demonstration of Continuous Electronic Structure Tuning via Strain in Atomically Thin MoS2. *Nano Lett.* **2013**, *13* (6), 2931−2936.

(6) Feng, J.; Qian, X.; Huang, C. W.; Li, J. Strain-Engineered Artificial Atom as a Broad-Spectrum Solar Energy Funnel. *Nature Photonics 2012 6:12* **2012**, *6* (12), 866−872.

(7) Castellanos-Gomez, A.; Roldán, R.; Cappelluti, E.; Buscema, M.; Guinea, F.; Van Der Zant, H. S. J.; Steele, G. A. Local Strain Engineering in Atomically Thin MoS2. *Nano Lett.* **2013**, *13* (11), 5361−5366.

(8) Dirnberger, F.; Ziegler, J. D.; Faria Junior, P. E.; Bushati, R.; Taniguchi, T.; Watanabe, K.; Fabian, J.; Bougeard, D.; Chernikov, A.; Menon, V. M. Quasi-1D Exciton Channels in Strain-Engineered 2D Materials. *Sci. Adv.* **2021**, *7* (44), 3066−3095.

(9) Lloyd, D.; Liu, X.; Christopher, J. W.; Cantley, L.; Wadehra, A.; Kim, B. L.; Goldberg, B. B.; Swan, A. K.; Bunch, J. S. Band Gap Engineering with Ultralarge Biaxial Strains in Suspended Monolayer MoS2. *Nano Lett.* **2016**, *16* (9), 5836−5841.

(10) Conley, H. J.; Wang, B.; Ziegler, J. I.; Haglund, R. F.; Pantelides, S. T.; Bolotin, K. I. Bandgap Engineering of Strained Monolayer and Bilayer MoS2. *Nano Lett.* **2013**, *13* (8), 3626−3630.

(11) Moon, H.; Grosso, G.; Chakraborty, C.; Peng, C.; Taniguchi, T.; Watanabe, K.; Englund, D. Dynamic Exciton Funneling by Local Strain Control in a Monolayer Semiconductor. *Nano Lett.* **2020**, *20* (9), 6791−6797.

(12) Johari, P.; Shenoy, V. B. Tuning the Electronic Properties of Semiconducting Transition Metal Dichalcogenides by Applying Mechanical Strains. *ACS Nano* **2012**, *6* (6), 5449−5456.

(13) Koo, Y.; Kim, Y.; Choi, S. H.; Lee, H.; Choi, J.; Lee, D. Y.; Kang, M.; Lee, H. S.; Kim, K. K.; Lee, G.; Park, K. D. Tip-Induced Nano-Engineering of Strain, Bandgap, and Exciton Funneling in 2D Semiconductors. *Adv. Mater.* **2021**, *33* (17), 2008234.

(14) Cordovilla Leon, D. F.; Li, Z.; Jang, S. W.; Cheng, C. H.; Deotare, P. B. Exciton Transport in Strained Monolayer WSe2. *Appl. Phys. Lett.* **2018**, *113* (25), 252101.

(15) Raja, A.; Chaves, A.; Yu, J.; Arefe, G.; Hill, H. M.; Rigosi, A. F.; Berkelbach, T. C.; Nagler, P.; Schüller, C.; Korn, T.; Nuckolls, C.; Hone, J.; Brus, L. E.; Heinz, T. F.; Reichman, D. R.; Chernikov, A. Coulomb Engineering of the Bandgap and Excitons in Two-Dimensional Materials. *Nature Communications* **2017**, *8* (1), 1−7.

(16) Borghardt, S.; Tu, J. S.; Winkler, F.; Schubert, J.; Zander, W.; Leosson, K.; Kardynał, B. E. Engineering of Optical and Electronic Band Gaps in Transition Metal Dichalcogenide Monolayers through External Dielectric Screening. *Phys. Rev. Mater.* **2017**, *1* (5), No. 054001.

(17) Lin, Y.; Ling, X.; Yu, L.; Huang, S.; Hsu, A. L.; Lee, Y. H.; Kong, J.; Dresselhaus, M. S.; Palacios, T. Dielectric Screening of Excitons and Trions in Single-Layer MoS2. *Nano Lett.* **2014**, *14* (10), 5569−5576.

(18) Gupta, G.; Kallatt, S.; Majumdar, K. Direct Observation of Giant Binding Energy Modulation of Exciton Complexes in Monolayer MoS E2. *Phys. Rev. B* **2017**, *96* (8), No. 081403.

(19) Ugeda, M. M.; Bradley, A. J.; Shi, S. F.; Da Jornada, F. H.; Zhang, Y.; Qiu, D. Y.; Ruan, W.; Mo, S. K.; Hussain, Z.; Shen, Z. X.; Wang, F.; Louie, S. G.; Crommie, M. F. Giant Bandgap Renormalization and Excitonic Effects in a Monolayer Transition Metal Dichalcogenide Semiconductor. *Nature Materials 2014 13:12* **2014**, *13* (12), 1091−1095.

(20) Utama, M. I. B.; Kleemann, H.; Zhao, W.; Ong, C. S.; da Jornada, F. H.; Qiu, D. Y.; Cai, H.; Li, H.; Kou, R.; Zhao, S.; Wang, S.; Watanabe, K.; Taniguchi, T.; Tongay, S.; Zettl, A.; Louie, S. G.; Wang, F. A Dielectric-Defined Lateral Heterojunction in a Monolayer Semiconductor. *Nature Electronics 2019 2:2* **2019**, *2* (2), 60−65.

(21) Stier, A. V.; Wilson, N. P.; Clark, G.; Xu, X.; Crooker, S. A. Probing the Influence of Dielectric Environment on Excitons in Monolayer WSe2: Insight from High Magnetic Fields. *Nano Lett.* **2016**, *16* (11), 7054−7060.

(22) Cho, Y.; Berkelbach, T. C. Environmentally Sensitive Theory of Electronic and Optical Transitions in Atomically Thin Semiconductors. *Phys. Rev. B* **2018**, *97* (4), No. 041409.

(23) Utama, M. I. B.; Kleemann, H.; Zhao, W.; Ong, C. S.; da Jornada, F. H.; Qiu, D. Y.; Cai, H.; Li, H.; Kou, R.; Zhao, S.; Wang, S.; Watanabe, K.; Taniguchi, T.; Tongay, S.; Zettl, A.; Louie, S. G.; Wang, F. A Dielectric-Defined Lateral Heterojunction in a Monolayer Semiconductor. *Nature Electronics 2019 2:2* **2019**, *2* (2), 60−65.

(24) Stier, A. V.; Wilson, N. P.; Clark, G.; Xu, X.; Crooker, S. A. Probing the Influence of Dielectric Environment on Excitons in

Monolayer WSe2: Insight from High Magnetic Fields. *Nano Lett.* **2016**, *16* (11), 7054−7060.
(25) Waldecker, L.; Raja, A.; Rösner, M.; Steinke, C.; Bostwick, A.; Koch, R. J.; Jozwiak, C.; Taniguchi, T.; Watanabe, K.; Rotenberg, E.; Wehling, T. O.; Heinz, T. F. Rigid Band Shifts in Two-Dimensional Semiconductors through External Dielectric Screening. *Phys. Rev. Lett.* **2019**, *123*, 206403.
(26) Chen, J. W.; Lo, S. T.; Ho, S. C.; Wong, S. S.; Vu, T. H. Y.; Zhang, X. Q.; Liu, Y. De; Chiou, Y. Y.; Chen, Y. X.; Yang, J. C.; Chen, Y. C.; Chu, Y. H.; Lee, Y. H.; Chung, C. J.; Chen, T. M.; Chen, C. H.; Wu, C. L. A Gate-Free Monolayer WSe2 Pn Diode. *Nature Communications 2018 9:1* **2018**, *9* (1), 1−7.
(27) Xiao, Z.; Song, J.; Ferry, D. K.; Ducharme, S.; Hong, X. Ferroelectric-Domain-Patterning-Controlled Schottky Junction State in Monolayer MoS2. *Phys. Rev. Lett.* **2017**, *118* (23), 236801.
(28) Zhao, P.; Kiriya, D.; Azcatl, A.; Zhang, C.; Tosun, M.; Liu, Y. S.; Hettick, M.; Kang, J. S.; McDonnell, S.; Kc, S.; Guo, J.; Cho, K.; Wallace, R. M.; Javey, A. Air Stable P-Doping of WSe2 by Covalent Functionalization. *ACS Nano* **2014**, *8* (10), 10808−10814.
(29) Fang, H.; Chuang, S.; Chang, T. C.; Takei, K.; Takahashi, T.; Javey, A. High-Performance Single Layered WSe 2 p-FETs with Chemically Doped Contacts. *Nano Lett.* **2012**, *12* (7), 3788−3792.
(30) Xu, Y.; Horn, C.; Zhu, J.; Tang, Y.; Ma, L.; Li, L.; Liu, S.; Watanabe, K.; Taniguchi, T.; Hone, J. C.; Shan, J.; Mak, K. F. Creation of Moiré Bands in a Monolayer Semiconductor by Spatially Periodic Dielectric Screening. *Nature Materials 2021 20:5* **2021**, *20* (5), 645−649.
(31) Su, H.; Xu, D.; Cheng, S.-W.; Li, B.; Liu, S.; Watanabe, K.; Taniguchi, T.; Berkelbach, T. C.; Hone, J. C.; Delor, M. Dark-Exciton Driven Energy Funneling into Dielectric Inhomogeneities in Two-Dimensional Semiconductors. *Nano Lett.* **2022**, *22*, 2843−2850.
(32) Wang, Q. H.; Kalantar-Zadeh, K.; Kis, A.; Coleman, J. N.; Strano, M. S. Electronics and Optoelectronics of Two-Dimensional Transition Metal Dichalcogenides. *Nature Nanotechnology 2012 7:11* **2012**, *7* (11), 699−712.
(33) Radisavljevic, B.; Radenovic, A.; Brivio, J.; Giacometti, V.; Kis, A. Single-Layer MoS2 Transistors. *Nature Nanotechnology 2011 6:3* **2011**, *6* (3), 147−150.
(34) Chhowalla, M.; Jena, D.; Zhang, H. Two-Dimensional Semiconductors for Transistors. *Nature Reviews Materials* **2016**, *1* (11), 1−15.
(35) Manzeli, S.; Ovchinnikov, D.; Pasquier, D.; Yazyev, O. V.; Kis, A. 2D Transition Metal Dichalcogenides. *Nature Reviews Materials* **2017**, *2* (8), 1−15.
(36) Chernikov, A.; Berkelbach, T. C.; Hill, H. M.; Rigosi, A.; Li, Y.; Aslan, O. B.; Reichman, D. R.; Hybertsen, M. S.; Heinz, T. F. Exciton Binding Energy and Nonhydrogenic Rydberg Series in Monolayer WS2. *Phys. Rev. Lett.* **2014**, *113* (7), No. 076802.
(37) Wang, G.; Chernikov, A.; Glazov, M. M.; Heinz, T. F.; Marie, X.; Amand, T.; Urbaszek, B. Colloquium: Excitons in Atomically Thin Transition Metal Dichalcogenides. *Rev. Mod. Phys.* **2018**, *90* (2), No. 021001.
(38) Berkelbach, T. C.; Hybertsen, M. S.; Reichman, D. R. Theory of Neutral and Charged Excitons in Monolayer Transition Metal Dichalcogenides. *Phys. Rev. B* **2013**, *88*, 45318.
(39) Gelly, R. J.; Renaud, D.; Liao, X.; Pingault, B.; Bogdanovic, S.; Scuri, G.; Watanabe, K.; Taniguchi, T.; Urbaszek, B.; Park, H.; Lončar, M. Probing Dark Exciton Navigation through a Local Strain Landscape in a WSe2Monolayer. *Nature Communications* **2022**, *13* (1), 1−7.
(40) Rosati, R.; Schmidt, R.; Brem, S.; Perea-Causín, R.; Niehues, I.; Kern, J.; Preuß, J. A.; Schneider, R.; Michaelis de Vasconcellos, S.; Bratschitsch, R.; Malic, E. Dark Exciton Anti-Funneling in Atomically Thin Semiconductors. *Nature Communications* **2021**, *12* (1), 1−7.
(41) Albagami, A.; Ambardar, S.; Hrim, H.; Sahoo, P. K.; Emirov, Y.; Gutiérrez, H. R.; Voronine, D. V. Tip-Enhanced Photoluminescence of Freestanding Lateral Heterobubbles. *ACS Appl. Mater. Interfaces* **2022**, *14* (8), 11006−11015.
(42) Ambardar, S.; Kamh, R.; Withers, Z. H.; Sahoo, P. K.; Voronine, D. V. Coupling Nanobubbles in 2D Lateral Heterostructures. *Nanoscale* **2022**, *14* (22), 8050−8059.
(43) Koo, Y.; Kim, Y.; Choi, S. H.; Lee, H.; Choi, J.; Lee, D. Y.; Kang, M.; Lee, H. S.; Kim, K. K.; Lee, G.; Park, K. D. Tip-Induced Nano-Engineering of Strain, Bandgap, and Exciton Funneling in 2D Semiconductors. *Adv. Mater.* **2021**, *33* (17), 2008234.
(44) Robertson, J. High Dielectric Constant Oxides. *European Physical Journal Applied Physics* **2004**, *28* (3), 265−291.
(45) Utama, M. I. B.; Kleemann, H.; Zhao, W.; Ong, C. S.; da Jornada, F. H.; Qiu, D. Y.; Cai, H.; Li, H.; Kou, R.; Zhao, S.; Wang, S.; Watanabe, K.; Taniguchi, T.; Tongay, S.; Zettl, A.; Louie, S. G.; Wang, F. A Dielectric-Defined Lateral Heterojunction in a Monolayer Semiconductor. *Nature Electronics 2019 2:2* **2019**, *2* (2), 60−65.
(46) Peña, T.; Chowdhury, S. A.; Azizimanesh, A.; Sewaket, A.; Askari, H.; Wu, S. M. Strain Engineering 2D MoS2 with Thin Film Stress Capping Layers. *2d Mater.* **2021**, *8* (4), No. 045001.
(47) Schnedermann, C.; Sung, J.; Pandya, R.; Verma, S. D.; Chen, R. Y. S.; Gauriot, N.; Bretscher, H. M.; Kukura, P.; Rao, A. Ultrafast Tracking of Exciton and Charge Carrier Transport in Optoelectronic Materials on the Nanometer Scale. *J. Phys. Chem. Lett.* **2019**, *10* (21), 6727−6733.
(48) Ashoka, A.; Gauriot, N.; Girija, A. V.; Sawhney, N.; Sneyd, A. J.; Watanabe, K.; Taniguchi, T.; Sung, J.; Schnedermann, C.; Rao, A. Direct Observation of Ultrafast Singlet Exciton Fission in Three Dimensions. *Nature Communications* **2022**, *13* (1), 1−8.
(49) Yuan, L.; Huang, L. Exciton Dynamics and Annihilation in WS 2 2D Semiconductors. *Nanoscale* **2015**, *7* (16), 7402−7408.
(50) Kumar, N.; Cui, Q.; Ceballos, F.; He, D.; Wang, Y.; Zhao, H. Exciton-Exciton Annihilation in MoSe 2 Monolayers. *Phys. Rev. B Condens Matter Mater. Phys.* **2014**, *89* (12), 125427.
(51) Sun, D.; Rao, Y.; Reider, G. A.; Chen, G.; You, Y.; Brézin, L.; Harutyunyan, A. R.; Heinz, T. F. Observation of Rapid Exciton-Exciton Annihilation in Monolayer Molybdenum Disulfide. *Nano Lett.* **2014**, *14* (10), 5625−5629.
(52) Li, Y.; Chernikov, A.; Zhang, X.; Rigosi, A.; Hill, H. M.; van der Zande, A. M.; Chenet, D. A.; Shih, E.-M.; Hone, J.; Heinz, T. F. Measurement of the Optical Dielectric Function of Monolayer Transition-Metal Dichalcogenides. *Phys. Rev. B* **2014**, *90*, 205422.
(53) Steinleitner, P.; Merkl, P.; Nagler, P.; Mornhinweg, J.; Schü, C.; Korn, T.; Chernikov, A.; Huber, R. Direct Observation of Ultrafast Exciton Formation in a Monolayer of WSe 2. *Nano Lett.* **2017**, *17*, 1455.
(54) Cadiz, F.; Robert, C.; Courtade, E.; Manca, M.; Martinelli, L.; Taniguchi, T.; Watanabe, K.; Amand, T.; Rowe, A. C. H.; Paget, D.; Urbaszek, B.; Marie, X. Exciton Diffusion in WSe2Monolayers Embedded in a van Der Waals Heterostructure. *Appl. Phys. Lett.* **2018**, *112* (15), 152106.
(55) Zipfel, J.; Kulig, M.; Perea-Causín, R.; Brem, S.; Ziegler, J. D.; Rosati, R.; Taniguchi, T.; Watanabe, K.; Glazov, M. M.; Malic, E.; Chernikov, A. Exciton Diffusion in Monolayer Semiconductors with Suppressed Disorder. *Phys. Rev. B* **2020**, *101* (11), 115430.
(56) Yu, Y.; Yu, Y.; Li, G.; Puretzky, A. A.; Geohegan, D. B.; Cao, L. Giant Enhancement of Exciton Diffusivity in Two-Dimensional Semiconductors. *Sci. Adv.* **2020**, *6* (51), 1.
(57) Kulig, M.; Zipfel, J.; Nagler, P.; Blanter, S.; Schüller, C.; Korn, T.; Paradiso, N.; Glazov, M. M.; Chernikov, A. Exciton Diffusion and Halo Effects in Monolayer Semiconductors. *Phys. Rev. Lett.* **2018**, *120* (20), 207401.
(58) Wagner, K.; Zipfel, J.; Rosati, R.; Wietek, E.; Ziegler, J. D.; Brem, S.; Perea-Causín, R.; Taniguchi, T.; Watanabe, K.; Glazov, M. M.; Malic, E.; Chernikov, A. Nonclassical Exciton Diffusion in Monolayer WSe 2. *Phys. Rev. Lett.* **2021**, *127*, 076801.
(59) Goh, K. E. J.; Lau, C. S.; Chee, J. Y.; Ang, Y. S.; Tong, S. W.; Cao, L.; Ooi, Z. E.; Wang, T.; Ang, L. K.; Wang, Y.; Chhowalla, M. Quantum Transport in Two-Dimensional WS2 with High-Efficiency Carrier Injection through Indium Alloy Contacts. *ACS Nano* **2020**, *14* (10), 13700−13708.

https://doi.org/10.1021/acsnano.3c05957
ACS Nano 2024, 18, 264−271

(60) Castellanos-Gomez, A.; Buscema, M.; Molenaar, R.; Singh, V.; Janssen, L.; Van Der Zant, H. S. J.; Steele, G. A. Deterministic Transfer of Two-Dimensional Materials by All-Dry Viscoelastic Stamping. *2d Mater.* **2014**, *1* (1), No. 011002.

https://doi.org/10.1021/acsnano.3c05957
ACS Nano 2024, 18, 264−271